

How old are places we've never been to?

Aiden Rolfe and Harry Gully (50/50 work)

November 2020

Abstract

In this project we will be exploring a method for determining the age of the Moon. Our chosen method was crater counting and ellipse fitting based on the paper Jain et al. (2013). We will first take you through a bit of theory on the topic of crater counting and why it is effective. Then, we will show you step-by-step how we performed the process of counting, using a combination of morphological image processing and image analysis, as well as how we went on to calculate an age for the Moon. We used 12 images of the Moon, each of which cover roughly 500 km^2 to $2,000 \text{ km}^2$ of the surface area. These images were taken from the Lunar Reconnaissance Orbiter Camera (LROC). The data collected from these images was fit to a production function of the Moon, taken from Neukum et al. (2001). From our data we calculated an age for the Moon of $3.93^{+0.06}_{-0.11}$ Gyr.

1 Introduction

1.1 Crater counting

One of the main purposes of crater counting and detection is to avoid hazards when landing spacecraft on the surfaces of celestial bodies. The first examples came in the time of the space race, where landing sites on the Lunar surface had to be predetermined to enable the safe landing in 1969. Another purpose of crater detection is optical landmark navigation which uses known craters to navigate spacecraft. In this paper, we use crater detection and counting to estimate the ages of celestial bodies.

No matter what the purpose, all crater counting and detection algorithms use similar techniques. These techniques have developed from the simple, manual detection of craters to the (semi-)automatic detection algorithms. Some of the previously attempted techniques have been unsatisfactory, however. Previous approaches have tried using template matching, a method of matching small parts of an image with a template image (Flores-Méndez 2003; Magee et al. 2003; Michael 2003; Saraiva et al. 2006). Other approaches have used texture analysis to identify objects within images (Barata et al. 2004; Kim et al. 2005). One approach even used the Hough Transform which extracts features in images using a voting procedure (Vinogradova et al. 2002). None of these approaches were adopted by the planetary science community due to the results simply not being good enough (Bandeira et al. 2007). We therefore follow a more recent method of automatic crater detection, developed by Jain et al. (2013). This method is explained thoroughly in section 2, alongside the reasoning of why each step in the method is taken.

Our goal of estimating ages of celestial bodies leads us to the study of the size-frequency distributions of lunar craters. In particular, the paper by Neukum et al. (2001) describes the relative stability of these derived distributions which are used to model cratering chronology. These chronology models show the relationship between crater frequency and age of the lunar surface. They are derived using decades of data which show different periods in the Moon's history. The ancient period of late-heavy bombardment was more than 3Gyr ago, where the crater projectile flux was highest, until it decayed into a relatively constant flux in the previous 3Gyr. The cratering chronology models also take into account resurfacing of the lunar surface, a process in which the surface evolves which removes evidence of previous impact craters. These models are used to derive the Lunar Production Function, explained in the next section.

1.2 Production Function

The production function, specifically, the production function of a celestial body, describes the relationship between the relative cratering rate and age of said body.

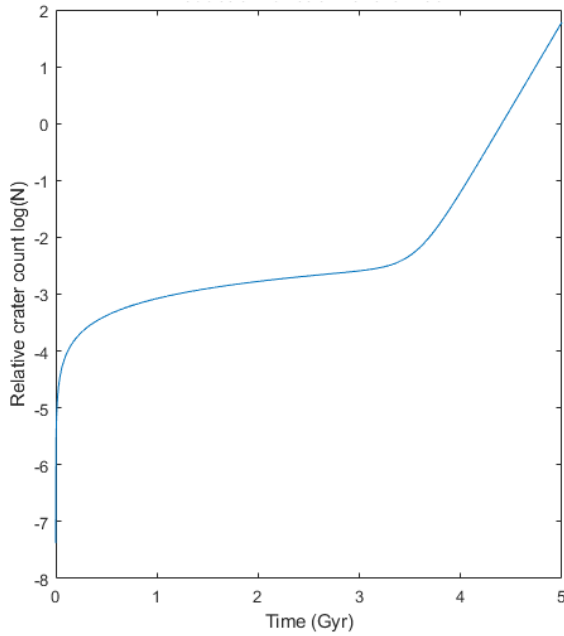


Figure 1: This plot shows the form of the production function of the Moon using equation 5 from Neukum et al. (2001). The x-axis reflects the age of the relative cratering area. The y-axis represents the relative crater count for said region. The y-axis was plotted using a log scale, as seen in Neukum et al. (2001) Figure 11. This is what we used to interpolate ages for different regions of the Moon.

The production function we used in this project, for the Moon, was

$$N = 5.44 \times 10^{-14} (e^{6.93T} - 1) + 8.38 \times 10^{-4}T \quad (1)$$

where N is the relative cratering rate and T is the estimated age of the region based on the cratering events (in Gyrs). This equation was taken from equation 5 of Neukum et al. (2001) and is shown by the plot in Figure 1.

As you can see from the graph in Figure 1, the early and late stages of the plot are fairly steep, which means small deviations in the relative crater count for those areas will not drastically affect the end result. However, the mid region is extremely shallow, thus creating a huge affect on the age interpolated when deviating from the intended relative crater count.

2 Method

As previously mentioned, there are different ways of automatically detecting craters in images. In this paper, we follow a similar method to the one laid out in Jain et al. (2013). We begin by smoothing the image using a combination of morphology opening and closing to discard the unwanted features of the image. We then apply a morphology gradient operation which detects the circular edges of the craters by using a combination of eroding and dilating. Following this, we produce a binary image by applying a global threshold to separate the pixels at the edge of the craters and the background pixels. This allows us to fit ellipses to the detected edges, which can then be used to count the craters.

2.1 Morphological Smoothing

The raw images we used had noise and other unwanted information, such as hills. The first step to filtering out this information is by smoothing the image. Before this, however, the image was converted from RGB to greyscale. The smoothing procedure we used was morphological, which is a mathematical way of processing geometrical structures. The process is a linear combination of opening and closing. Morphology opening removes brighter pixels, which are generally small objects found in the image. This is done by eroding the image, then dilating the eroded image. Closing the image removes small holes. In a similar manner to opening, the image is dilated. Then, the dilated image is eroded. In the context of morphology, erosion involves adjusting pixels to the minimum value of all neighbouring pixels. Dilation adjusts the pixels to the maximum value of neighbouring pixels. Figure 2 shows the process of smoothing visually.

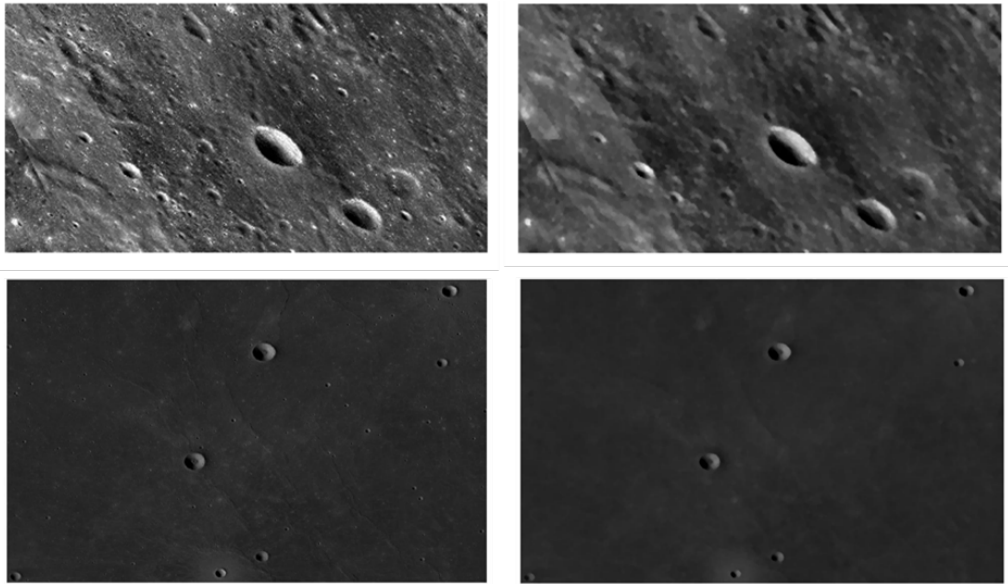


Figure 2: The two images on the left hand side were taken from the Lunar Reconnaissance Orbiter Camera. The images were converted to greyscale before any other processing was performed. The images on the right show the respective results after applying morphology opening and closing. The structuring element used here was a disk of size 8. This was chosen to exaggerate the effect of the smoothing process.

Figure 2 mentions the use of a structuring element. The structuring element is a shape used to compare with other shapes found on the image you are probing. For the purpose of crater detection, this is useful for finding shapes, or craters in this case, which are greater than a certain size (Jain et al. 2013). The structuring element is used for both the opening and the closing. In each case, it is best to use the same structuring element. Another smoothing method, such as the Gaussian blur, would smooth everything in the image, even the useful parts. This is the advantage of this method. It allows us to keep more useful information for this specific applications. Craters were the objects we were wanting to keep in the images, so, a disk shaped structuring element was the most suitable choice. In Figure 2, the size of the structuring element used was 8. This was done to emphasize the effect of smoothing. However, for the purpose of crater detection, specifically with images taken from the Lunar Reconnaissance Orbiter Camera (LROC), we found a structuring element of size 4 to be the most effective across the board. This was determined through trial and error until the crater count was most accurate.

2.2 Morphology Gradient

This process follows on from the smoothing stage. The gradient procedure is applied to the already smoothed image. The morphology gradient is the difference between the dilation and the erosion of an image. It is as simple as calculating the erosion of the image and subtracting it from the dilation. Dilation and erosion in this case are the same processes I described in **2.1**. The result of calculating the gradient is shown in Figure 3.

Just like with the smoothing, a structuring element is used. The structuring element of choice does not necessarily have to be the same one used in the smoothing process. Sticking with the disk shaped element, we found that an element of size 7 was very effective for most, if not all of our images. The morphology gradient has removed a lot of information from the smoothed image. By using the disk structuring element, the circular features of the image are pulled out, however, there is still some unwanted noise. The image still needs to be processed more before we can start counting the craters.

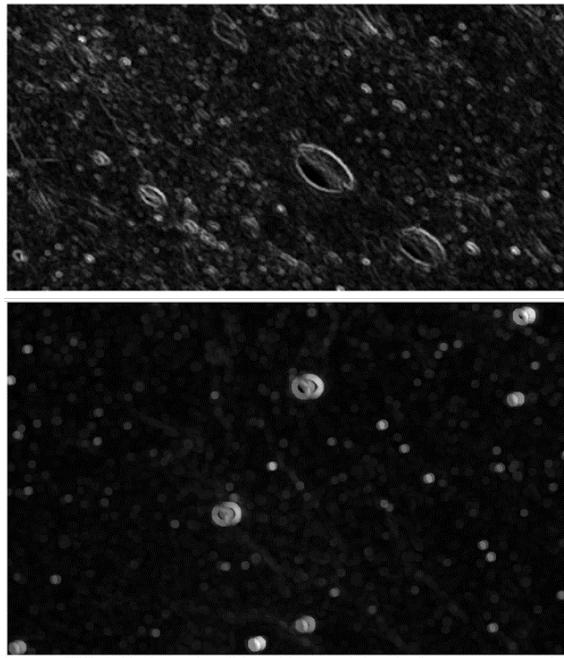


Figure 3: Following on from Figure 2, this is the result of calculating the morphology gradient of the already smoothed images. (*Top*: first row in Figure 2, *Bottom*: second row in Figure 2). In this particular example, a disk structuring element of size 7 was used. A lot of the unwanted data has been removed from the image, making processes like edge detection much easier.

2.3 Binarization and Ellipse Fitting

Applying the gradient operation to the smoothed image detects the circular edges of the craters. As you can see in Figure 3, the edges of the craters are clearly detected. However, there are other, unwanted, features in the image. If ellipses were fitted to the image at this stage, there would be many false detections. To overcome this, a global threshold is applied in order to segment the image into the edges and the background. Deciding what value to use for the threshold wasn't a simple choice as each image is different. To get an idea of where the threshold should be

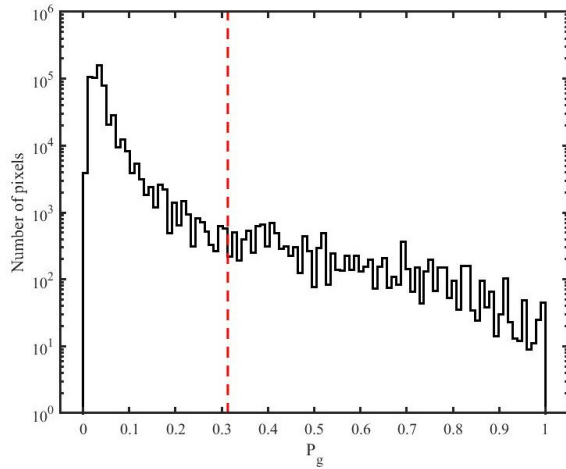


Figure 4: A histogram of the pixel grey values from the bottom image in Figure 3 (black line) in a log scale, and the chosen threshold value, given by equation 2 (red dashed line).

placed, we plotted a histogram of the pixel values from the bottom image in Figure 3 . As you can see in Figure 4, the vast majority of pixels are dark (i.e. background pixels). We started by selecting an arbitrary value for the threshold, then comparing that value to the mean and standard deviation of the pixel values. This led us to the equation

$$t = \bar{P}_g + X\sigma_p \quad (2)$$

where t is the threshold value, \bar{P}_g is the mean pixel value, σ_p is the standard deviation of the pixel values, and X is some constant. This enabled us to use different threshold values for each image, meaning we could cater to the differing pixel values in each image. This also kept our method automatic, rather than having to manually select a threshold value for each image. Selecting a value for the constant X however, was manual. We approached this in a similar way to how we approached the choice of shape and size of the structuring elements used in the previous sections. Eventually, we settled on a value of $X = 3.12$ as this struck the best balance between detecting as many craters as possible, whilst keeping false detections to a minimum.

Upon selecting a threshold value for each image automatically, we then set all pixels above this threshold to 1, and all those below to 0, thus producing a binary image (shown in Figure 5).

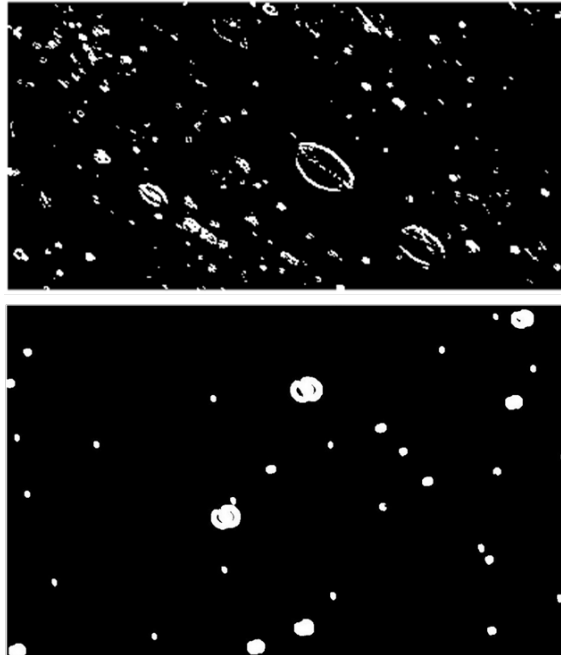


Figure 5: The result of binarization of the images in Figure 3 after applying a global threshold of 0.29. This allows us to move onto the next step of ellipse fitting.

Figure 5 clearly shows the different regions, where each white blob represents a different crater. As our goal is to only find the number of craters in a given image, we don't necessarily need to fit ellipses to the regions found in Figure 5. However, to be able to compare the detected craters to the craters we can see, we applied a simple ellipse fitting technique to the image. This works by finding the centres of contiguous, 8-connected white regions in the image. This means it will start by finding a white pixel, then labelling all white pixels neighbouring that pixel as the same region. This allows measurements of the semi major and minor axes of the ellipses to be found as well as the centres of the regions. Once the whole image is scanned and all contiguous regions are found, we overlaid the ellipses onto the original image. This is shown in Figure 6.

The only craters not detected are the very small ones. There had to be a cut-off point on the sizes of the detected craters as, the more you zoom in on the image, the more small craters you will find. This cut-off point is altered by the choice in the size of the structuring element used in section 2.1, as any craters smaller than this structuring element will not be detected. As explained previously, we chose the size that gave us the best balance between detecting the highest number of craters, and minimising the number of false detections.

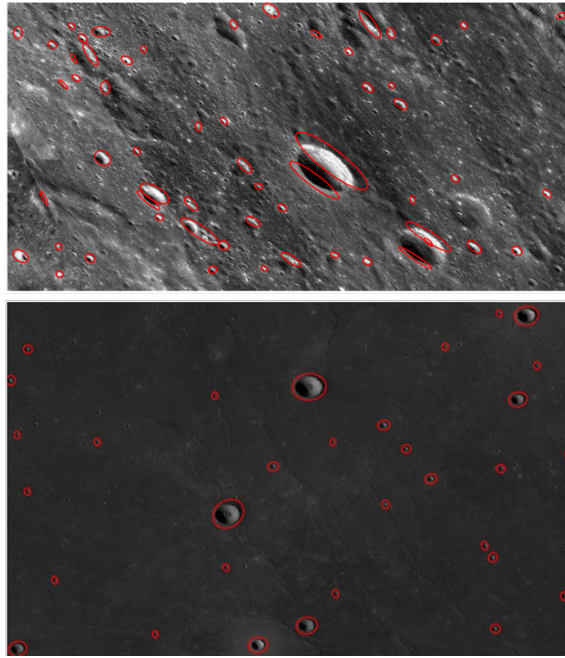


Figure 6: These are the ellipses which have been fitted to the binary images from Figure 5, overlaid on top of the original images from Figure 2.

3 Results

All images used were taken by the LROC. As a result, each image has a scale associated with it. These scales were given by a conversion factor (S_p) with units of meters per pixel. Therefore, the physical area of each image was calculated using the equation

$$A = \text{height} \times \text{width} \times S_p^2 \quad (3)$$

where the *height* and *width* correspond to the height and width of the images in number of pixels. This area is given in units of m^2 so a simple conversion to km^2 was applied.

One aspect we had to consider when choosing the images to use was the size of the area on the Moon we analyse in each picture. To begin with, we performed crater counting on a very large area of the Moon (roughly in the $100,000\ km^2$ to $1,000,000\ km^2$ range). 6 images in this range were analysed and an age of 0.03 ± 0.01 Gyrs with a 1σ error was found. This value was quite far from the one we were expecting, so we reconsidered our choice of images to perform the count on, and decided to use smaller surface areas. In this case, what we refer to as a small surface area are surface areas in the approximate range of $500\ km^2$ to $2,000\ km^2$. It was clear that this range yielded much more sensible results, so we proceeded using this scale of image.

The simple explanation for this is the fact that the more you zoom out on the surface map of the Moon, provided by the LROC, the more detail you lose. Too much information is lost when looking at such a large area. Relative to a surface area in the $1,000,000\ km^2$ range, a huge amount of craters will not be seen. Figure 7 compares two images of the Moon with vastly different surface areas. The difference in the conditions of each image reflects how different the results each image provides, using the same method. The image on the left with a larger surface area does not accurately depict the number of craters found in said area.

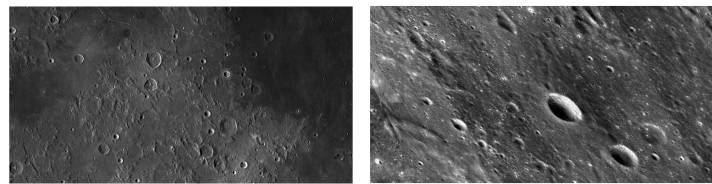


Figure 7: On the left is an image of the Moon covering a surface area of roughly $1,400,000\ km^2$. On the right is another image of the Moon covering roughly $1,700\ km^2$.

We applied the method laid out in section 2 to 12 individual images taken by the LROC. For each image, the number of detected craters were counted ($N_{craters}$), as well as the physical area, given by equation (3). We were then able to calculate the N value, from equation (1), for each image, using the equation

$$N = \frac{N_{craters}}{A} \quad (4)$$

where N is given in units of km^{-2} . To get as accurate a result as possible for the age of the Moon, we combined the N values for each image into a mean value \bar{N} . The results for each image are laid out in Table 1. We find the average number of craters per km^2 to be $\bar{N} = 0.04 \pm 0.02 km^{-2}$ where the error is calculated using the standard deviation of the N values.

To calculate the age of the Moon, we need to solve equation (1) with our value of \bar{N} . We do this for the entire error range as well, which gives us a range for the age of the Moon. The result is shown in Figure 8.

Table 1: The cratering information for each of the chosen images.

Image	$N_{craters}$	Area (km^2)	$N (km^{-2})$
1	32	1348	0.02
2	26	838.4	0.03
3	30	954.4	0.03
4	22	696.0	0.03
5	35	1095	0.03
6	68	854.4	0.08
7	73	1614	0.05
8	112	1614	0.07
9	91	1614	0.06
10	78	1685	0.05
11	67	1685	0.04
12	58	1685	0.03
Mean	~ 58	1307	^a 0.04 ± 0.02

Notes. ^aMean number of craters per km^2 with the associated 1σ error.

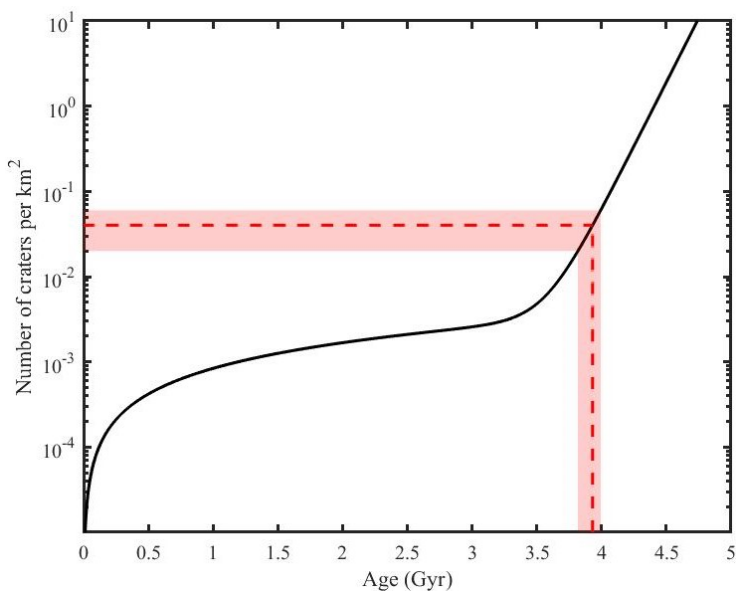


Figure 8: A plot of the Lunar Production Function given in equation (1) (black line) with the solutions for our value of \bar{N} (red dashed line) including the 1σ errors (red shaded area).

As shown in Figure 8, the average age of the Lunar surface, calculated from our 12 chosen images is $\bar{T} = 3.93^{+0.06}_{-0.11}$ Gyr. While the actual age of the Moon (4.53 Gyr) isn't within the 1σ error of our result, we are still reasonably close. This difference can be explained by examining the images in Figure 6 more closely. Even though we argue why the method used in this paper is better than other previous attempts, it is still impossible to detect 100% of the craters (shown in Figure 6). By detecting less craters than there actually are, the value of \bar{N} is less than it should be which then corresponds to a smaller age.

4 Conclusion

The goal of this project was to create a tool that can automatically detect craters on the surface of a celestial body, and use that to estimate an age of that surface. We have presented what we believe to be the best method of automatic crater detection - a method which involves 4 main steps: morphological smoothing in order to remove the unwanted features of an image, the morphology gradient procedure which detects the circular edges of craters, binarization which removes more unwanted features as well as allowing us to complete the next step, fitting ellipses to the detected craters in the image. We used this method to detect an average of 58 craters in 12 separate images, taken by the LROC, with an average area of 1307 km^2 . From this, an average cratering density was calculated which allowed us to find an average age of the surfaces, using the Lunar Production Function. Using this method, we estimate the average age of the surfaces of the 12 chosen images to be $3.93^{+0.06}_{-0.11}$ Gyr.

The method laid out in this paper can be extended to other celestial bodies, such as Mercury or Pluto. Our method of counting craters would stay the same for these different celestial bodies, however, the production function would have to be altered.

References

- Bandeira L.P.C., Saraiva J., Pina P. (2007) Development of a Methodology for Automated Crater Detection on Planetary Images. In: Martí J., Benedí J.M., Mendonça A.M., Serrat J. (eds) Pattern Recognition and Image Analysis. Ibpria 2007. Lecture Notes in Computer Science, vol 4477. Springer, Berlin, Heidelberg.
- Barata, T., Alves, E.I., Saraiva, J. and Pina, P., 2004, September. Automatic recognition of impact craters on the surface of Mars. In International Conference Image Analysis and Recognition (pp. 489-496). Springer, Berlin, Heidelberg.
- Flores-Méndez, A., 2003, November. Crater marking and classification using computer vision. In Iberoamerican Congress on Pattern Recognition (pp. 79-86). Springer, Berlin, Heidelberg.
- Jain, Amee. ‘Automatic crater detection on Lunar surface’ 2, no. 5 (2013): 6. 2013.
- Kim, J.R., Muller, J.P., van Gasselt, S., Morley, J.G. and Neukum, G., 2005. Automated crater detection, a new tool for Mars cartography and chronology. Photogrammetric Engineering Remote Sensing, 71(10), pp.1205-1217.
- Magee, M., Chapman, C.R., Dellenback, S.W., Enke, B., Merline, W.J. and Rigney, M.P., 2003. Automated identification of Martian craters using image processing. LPI, p.1756.
- Michael, G.G., 2003. Coordinate registration by automated crater recognition. Planetary and Space Science, 51(9-10), pp.563-568.
- Neukum, G., B.A. Ivanov, and W.K. Hartmann, “Cratering records in the inner solar system in relation to the lunar reference system”, Space Science Reviews, p. 55-86, 2001.
- Saraiva, J., Bandeira, L.P.C. and Pina, P., 2006. A structured approach to automated crater detection. LPI, p.1142.
- Vinogradova, T., Burl, M. and Mjolsness, E., 2002, March. Training of a crater detection algorithm for Mars crater imagery. In Proceedings, IEEE Aerospace Conference (Vol. 7, pp. 7-7). IEEE.